Pharm Res (2014) 31:1302–1314
DOI 10.1007/s11095-013-1251-9

RESEARCH PAPER

Chitosan-Based Polyelectrolyte Complexes as Potential Nanoparticulate Carriers: Physicochemical and Biological Characterization

Thiruganesh Ramasamy • Tuan Hiep Tran • Hyuk Jun Cho • Jeong Hwan Kim • Yong Il Kim • Jae Yoon Jeon • Han-Gon Choi • Chul Soon Yong • Jong Oh Kim

Received: 8 August 2013 / Accepted: 10 November 2013 / Published online: 3 December 2013

ABSTRACT

Purpose To investigate the effect of polyelectrolytes on the formation and physicochemical properties of chitosan nanoparticles (CS-NPs) used for the delivery of an anticancer drug, doxorubicin (DOX).

Method Three DOX-loaded CS-NPs were formulated with tripolyphosphate (CS-TP/DOX NPs), dextran sulfate (CS-DS/DOX NPs), and hyaluronic acid (CS-HA/DOX NPs) by using ionotropic gelation or complex coacervation.

Results CS-TP/DOX NPs were the smallest, with an average size of ~100 nm and a narrow size distribution, while CS-DS/DOX and CS-HA/DOX NPs were ~200 nm in size. Transmission electron microscopy clearly showed a spherical shape for all the NPs. The strong binding affinity of DOX for the multiple sulfate groups in DS resulted in a sustained release profile from CS-DS/DOX NPs at pH 7.4, while CS-HA/DOX NPs exhibited faster DOX release. This trend was also present under acidic conditions, where release of DOX was significantly augmented because of polymer protonation. Compared to CS-TP/DOX or CS-DS/DOX NPs, CS-HA/DOX NPs showed superior cellular uptake and cytotoxicity in MCF-7 and A-549 cells, because of their ability to undergo CD44-mediated endocytosis. Pharmacokinetic studies clearly showed that all CS-NPs tested significantly improved DOX plasma circulation time and decreased its elimination rate constant. Consistent with the *in vitro* release data, CS-DS/DOX NPs exhibited a relatively better DOX plasma profile and enhanced blood circulation, compared to CS-HA/DOX or CS-TP/DOX NPs. Overall, these results demonstrated how NP design can influence their function.

Conclusions Taken together, CS-based polyelectrolyte complexes could provide a versatile delivery system with enormous potential in the pharmaceutical and biomedical sectors.

KEY WORDS chitosan · dextran sulfate · hyaluronic acid · polyelectrolyte complex · tripolyphosphate

INTRODUCTION

Polymer-based nanoparticulate systems formulated via ionotropic gelation or coacervations are attracting attention owing to their simplicity and versatility (1). These colloidal polyelectrolyte complexes (PEC) are formed by the interaction of two or more oppositely charged macromolecules or ions. Generally, oppositely charged polyelectrolytes aggregate because of charge density fluctuation-induced electrostatic attraction (2). The formation and stability of PEC are influenced

Electronic supplementary material The online version of this article (doi:10.1007/s11095-013-1251-9) contains supplementary material, which is available to authorized users.

T. Ramasamy • T. H. Tran • H. J. Cho • J. H. Kim • Y. I. Kim • C. S. Yong (✉) • J. O. Kim (✉)
College of Pharmacy, Yeungnam University, 214-1, Dae-dong Gyeongsan 712-749, South Korea
e-mail: csyong@yu.ac.kr
e-mail: jongohkim@yu.ac.kr

H.-G. Choi (✉)
College of Pharmacy, Hanyang University, 55, Hanyangdaehak-ro Ansan 426-791, South Korea
e-mail: hangon@hanyang.ac.kr

J. Y. Jeon
Ernest Mario School of Pharmacy, Rutgers University New Brunswick, New Jersey 08854, USA

by many factors such as degree of ionization, charge distribution of the cationic and anionic counterparts, molecular weights of the polyelectrolytes, weight ratio of polymers, temperature, and interaction time (3, 4). In this milieu, delivery systems prepared from naturally derived polyelectrolytes have generated substantial research interest because of their biodegradability and biocompatibility.

Chitosan (CS) is a natural polysaccharide that has been extensively investigated by pharmaceutical and biomedical industries because of its high biocompatibility, as well as its biodegradability, and bioadhesive and cationic characteristics (5–7). CS has a pKa of around 6–6.5 and is therefore readily soluble in an acidic environment, because of protonation of the amine functional group in the glucosamine unit. The resulting positive charge on CS paves the way for ionotropic gelation/coacervation with an anionic counterpart (8–10). It has previously been reported that positively charged CS nanoparticles (NPs) exhibited stronger affinity towards the negatively charged cell membrane, resulting in higher cellular uptake (11). CS-NPs prepared via ionotropic gelation offer many advantages such as avoidance of organic solvent use, a simple production method, and augmented stability owing to ionic cross-linking (12, 13). In addition to these unique benefits, ionic cross-linking also helps avoid the use of chemical cross-linking agents and emulsifying agents that are not only toxic to cells but also affect the drug loading and biological properties (14, 15).

Although CS can form nano-sized particles, the choice of polyanion (anionic polymer) can greatly influence the size of the assembled NPs, *in vivo* stability, and cytotoxic effects. We therefore selected three of the most popular polyanions (tripolyphosphate [TP], dextran sulfate [DS], and hyaluronic acid [HA]) to form complexes with CS. The number of ionic groups interacting with the CS amine group will determine the NP characteristics. TP is an extensively studied multivalent cross-linking agent with a triple negative charge per residue throughout the physiological pH range (16). DS, a highly anionic and biocompatible polymer, comprises around 2.3 sulfate groups per glucosyl units with branching at 1–6 and 1–4 glycosidic linkages (6, 17). HA is another biocompatible anionic biopolymer naturally found in humans and used in a number of biomedical applications. In addition, HA interacts with cellular receptors (CD44, the hyaluronan-mediated motility receptor [RHAMM] and the hyaluronan receptor on liver endothelial cells [HARLEC]) expressed in human cancer cells, increasing drug specificity for these cells (18–20). Doxorubicin (DOX; pKa 8.2) was used as a model drug for encapsulation into these PEC NPs. The polyanionic charge present on the polymers was used to electrostatically bind the positively charged DOX. To the best of our knowledge, no attempts have been made to compare how polyanions influence the physicochemical properties of PEC NPs and DOX delivery from three different CS-NPs.

The purpose of this study was to understand the influence of different polyanions on the physicochemical and biological characteristics of CS-NPs. In particular, the study aimed to encapsulate DOX in TP, DS, and HA-based CS-NPs, and to observe the behavior of these NPs *in vitro* and *in vivo*. Two different human cancer cell lines (MCF-7 and A-549) were used to evaluate the cellular uptake and cytotoxicity of these three different CS-NPs.

MATERIALS AND METHODS

Materials

Doxorubicin (DOX) hydrochloride was a kind gift from Dong-A Pharmaceutical Company (Yongin City, South Korea). Chitosan (low molecular weight; viscosity 20–200 cps; degree of acetylation 85%), dextran sulfate sodium salt (MW; 5,000 Da) and MTT reagent (3-(4,5-dimethylthiazol-2-yl)-2,5-diphenyl tetrazolium bromide) were purchased from Sigma-Aldrich (St. Louis, MO. USA). Sodium tripolyphosphate was obtained from Daejung Chemicals & Metals Co., Ltd. (Seoul, South Korea). Hyaluronic acid (MW; 3,000 Da) was procured from B&K Technology Group Co., Ltd. (Xiamen, China). Fetal bovine serum (FBS) and Dulbecco's Modified Eagle's Medium (DMEM) were purchased from Invitrogen Inc. (Carlsbad, CA, USA). MCF-7 cell and A-549 cells were obtained from the Korean Cell Bank (Seoul, South Korea). All other chemicals were of reagent grade and were used as supplied.

Preparation of Polyanion-Based CS-NPs

Polyanion-based CS-NPs were prepared by ionotropic gelation or complex coacervation (13). CS solution was prepared in 0.5% (v/v) aqueous acetic acid solution and stirred overnight, followed by filtration through a 0.45 μm syringe filter. The final pH of the CS solution was adjusted to 5.5 with 0.1 M NaOH. TP, DS, and HA solutions (1 mg/mL) were prepared in distilled water, followed by filtration with a 0.2 μm syringe filter. The final pH of these anionic solutions was adjusted to 7.0. The anionic solutions (1 mg/mL) were added drop-wise into the CS solution (1 mg/mL) under magnetic stirring (1,000 rpm) at 25°C. Stirring was maintained and the mixture was allowed to cross-link for 45 min to enable complete stabilization of the system. Various molar ratios of CS and anionic solutions were investigated to obtain the smallest possible CS-TP NPs, CS-DS NPs, and CS-HA NPs.

DOX-loaded CS-NPs were prepared by firstly pre-mixing DOX solution and CS solution and incubating for 30 min. TP, DS, or HA solutions were then added, allowing competitive binding of DOX to the negatively charged polymer while forming the CS-TP/DOX NPs, CS-DS/DOX NPs, and CS-HA/DOX NPs.

Hydrodynamic Size, Polydispersity, and ζ-Potential Measurements

The hydrodynamic size, polydispersity index (PDI), and ζ-potential measurements were analyzed by dynamic light scattering (Nano-Z & Nano-S90 ZetaSizer; Malvern Instruments, UK). Measurements were performed at a fixed scattering angle of 90°. The NPs were suitably diluted with distilled water and measured at 25°C. The hydrodynamic size was determined using the Stokes-Einstein equation. The PDI and ζ-potential were determined from the manufacturer's software (version 6.34). Each measurement was performed using at least three sets of ten runs.

Morphological Analysis

The NP morphology was examined by transmission electron microscope (TEM) (H7600, Hitachi, Japan) at an accelerating voltage of 100 kV. A drop of NP dispersion was deposited on the copper grid and counterstained by 1% phosphotungstic acid prior to TEM imaging.

Drug Loading

Drug loading was evaluated using a colorimetric method. Unbound drug (DOX) was removed by ultrafiltration using an Amicon centrifugal filter device (MWCO 10,000 Da, Millipore), pretreated with DOX. The final concentration of DOX-loaded CS-NPs was determined by measuring the absorbance of the filtrate at 482 nm, using a spectrophotometer (Perkin Elmer U-2800, Hitachi, Japan).

Physical State Characterization

The surface chemistry and physical interaction between polymers and DOX were determined from Fourier transform infrared (FTIR) spectra. Samples for FTIR spectrometry were prepared in potassium bromide and analyzed over the 400–4,000 cm^{-1} range using a Bomen MB-II FTIR spectrometer (Hartmann & Brawn Co, USA). X-ray diffraction (XRD) patterns were also obtained using an X-ray diffractometer (X'Pert PRO MPD diffractometer, Almelo, The Netherlands) with a copper anode (Cu Kα radiation) operated at a voltage of 40 kV with a current of 30 mA radiation, scattered in the crystalline regions of the sample, and measured using a vertical goniometer. Patterns were obtained using a step width of 0.04°C with a detector resolution in 2θ (diffraction angle) between 10°C and 60°C.

In Vitro Release Study

The release of DOX from CS-TP/DOX NPs, CS-DS/DOX NPs and CS-HA/DOX NPs was evaluated in phosphate buffered saline (PBS, pH 7.4, 0.14 M NaCl), and in acetate buffered saline (pH 5.0, 0.14 M NaCl) by dialysis using membrane tubing (Spectra/Por®; 3,500 Da cutoff, CA, USA). The dialysis was performed at 37°C. The concentrations of DOX present in the dialysate were determined spectrophotometrically by measuring absorbance at 482 nm. The concentration of DOX released from the NPs was expressed as a percentage of the total drug available and plotted as a function of time.

Cellular Uptake Study

The cellular uptake of DOX from CS-TP/DOX NPs, CS-DS/DOX NPs, and CS-HA/DOX NPs was quantitatively analyzed using high performance liquid chromatography (HPLC). MCF-7 and A-549 cells (5×10^5) were seeded in 6-well plates and allowed to attach for 24 h. The cells were washed, treated with each type of NP (50 μg/mL) and incubated for 2 h at 37°C. Cells were then washed three times with PBS and treated with a trypsin/PBS mixture. The harvested cells were lysed by sonication (2 min), centrifuged (13,000 rpm) for 10 min, and 20 μL of supernatant was injected into the HPLC system for quantitative DOX analysis.

In Vitro Cytotoxicity Assay

The *in vitro* cytotoxicity of free DOX, CS-TP/DOX NPs, CS-DS/DOX NPs and CS-HA/DOX NPs was assessed by MTT assay as reported previously (21). Briefly, 1×10^4 MCF-7 cells or A-549 cells were seeded in 96-well plates and allowed to attach for 24 h. Cells were incubated with DOX or DOX-loaded CS NPs for 24 h at 37°C. The cells were then washed twice with PBS and maintained in DMEM medium with 10% FBS for an additional 72 h before adding 100 μL MTT (1.25 mg/mL) to each well and incubating for 3 h at 37°C in the dark. DMSO (100 μL) was added to each well to extract the formazan crystals, prior to measurement of the absorbance at 570 nm in a microplate reader (Multiskan EX, Thermo scientific, Finland). All measurements were taken eight times. The cell viability was calculated as $A_{sample}/A_{control} \times 100\%$.

Live/Dead Assay

Cytotoxicity was further visualized using the Live/Dead assay. MCF-7 or A-549 cells (5×10^5) were seeded in 6-well plates and allowed to attach for 24 h. Cells were exposed to CS-TP/DOX NPs, CS-DS/DOX NPs or CS-HA/DOX NPs for 6 h at 37°C. Cells were washed twice with PBS and stained with the Live/Dead assay kit (calcein AM and ethidium homodimer-1) for 20 min. The cells were washed twice with PBS and fixed with 4% paraformaldehyde for 10 min prior to visualization under a fluorescence microscope (TE2000-U,

Nikon; USA). Cells stained green reflected the proportion of live cells.

Pharmacokinetic Study

Study Protocols

Male Sprague–Dawley rats weighing 240±10 g were divided in 4 groups, with 3 rats in each group, and fasted for 12 h prior to the experiments. The protocols for the animal studies were approved by the Institutional Animal Ethical Committee, Yeungnam University, South Korea.

Administration and Blood Collection

The right femoral artery of each rat was cannulated to withdraw the blood samples (22). The left femoral vein was cannulated to allow administration of either free DOX solution, CS-TP/DOX NPs, CS-DS/DOX NPs or CS-HA/DOX NPs. The surgical openings were properly stitched with surgical thread to reduce pain and to maximize the study period. At predetermined intervals (0.25, 0.5, 1, 2, 4, 6, 8, 10, 12, and 24 h) 0.25 mL of blood was collected from the right femoral artery and immediately centrifuged (Eppendorf, Hauppauge, NY, USA) at 13,000 rpm for 10 min.

Blood Sample Analysis

150 μL of the plasma supernatant was mixed with 150 μL of acetonitrile and vortex-mixed for 30 min. The sample was then centrifuged at 13,000 rpm for 10 min. The supernatant was separated and evaporated at 40°C in a vacuum dryer (Modul 3180C, Buchon, South Korea). The residue was reconstituted in 100 μL of acetonitrile, vortex-mixed (3 min), and centrifuged. Twenty microliters of this supernatant was injected into the HPLC system to quantify plasma DOX level.

HPLC Conditions

Plasma DOX was analyzed using a Hitachi HPLC system consisting of a pump (Model L2100), an auto sampler (Model L2200) and an ultraviolet detector (Model L2420). A C_{18} analytic column (Inertsil® ODS3: 0.5 μm, 15 cm×0.46 cm, GL Sciences Inc., Japan) was used. The mobile phase consisted of methanol:water:acetic acid (50:49:1; pH 2.9) at a flow rate of 1.2 mL/min. The effluent was monitored at a UV absorption wavelength of 280 nm.

Pharmacokinetic Data Analysis and Statistical Analysis

The area under the drug concentration-time curve from 0 to 24 h (AUC), elimination rate constant (K_{el}) and half-life ($t_{1/2}$) were calculated using non-compartmental analysis (WinNonlin; professional edition, version 2.1; Pharsight Co., Mountain View, CA, USA). The peak concentration of drug (C_{max}) and the time taken to reach the peak concentration (T_{max}) were obtained directly from the plasma *vs*. time profile. Levels of statistical significance were assessed using analysis of variance (ANOVA). Differences were considered to be statistically significant when $p<0.05$. All data were expressed as mean ± S.D.

RESULTS AND DISCUSSION

Effect of Polymer Ratio on Hydrodynamic Size and Polydispersity

The effects of different polymer weight ratios on NP size and size distribution were investigated to find the optimum ratios for production of small stable CS-NPs with a narrow size distribution. Polymer weight ratio (w/w) is an important determinant of CS-NP properties, which in turn affect their biological performance. For instance, the PDI of CS-TP NPs was higher when a low TP concentration was used, whilst the NP size was reduced with a higher TP weight ratio (15) (Fig. 1a). This trend was reversed and NP size increased markedly with further addition of TP. As shown in Fig. 1a, the optimum ratio of CS to TP was 10:4. Similarly, the optimal CS to DS ratio for CS-DS NPs was 10:6 (Fig. 1b). However, CS-TP NPs were 105.3±1.5 nm, much smaller than CS-DS NPs (212.7±2.3 nm). In contrast to these TP and DS-based systems, CS-HA produced larger (256.0± 25.1 nm) stable NPs at much higher proportions of HA (CS:HA = 10:20) (Fig. 1c). This phenomenon was attributed to the presence of a high charge density in TP and DS, compared to the low or mono charge in HA.

In general, CS (pKa, ~6.5) is present in the collapsed state under basic conditions. However, under acidic conditions, it attains an expanded or swollen state, owing to the protonation of amino sugar moieties (23). In contrast, TP, DS, and HA remain de-protonated at basic pH, giving them a strong negative charge. The degree of ionization determines the charge density on each molecule and affects its CS binding affinity. Thus, it can be anticipated that when these two oppositely charged groups of polymers are mixed, negatively charged molecules self-assemble with positively charged CS via electrostatic interactions. The comparatively low molecular weight anionic molecules (1,000–5,000 Da), become interspersed between the large CS polymer chains (5). However, the size and stability of PEC formed in this way will depend upon the polymer charge density and the weight ratio between the two polymers (13).

Moreover, limited molecular aggregation takes place at low concentrations of anionic molecule. With increasing concentrations of counter ion, aggregation increases with the

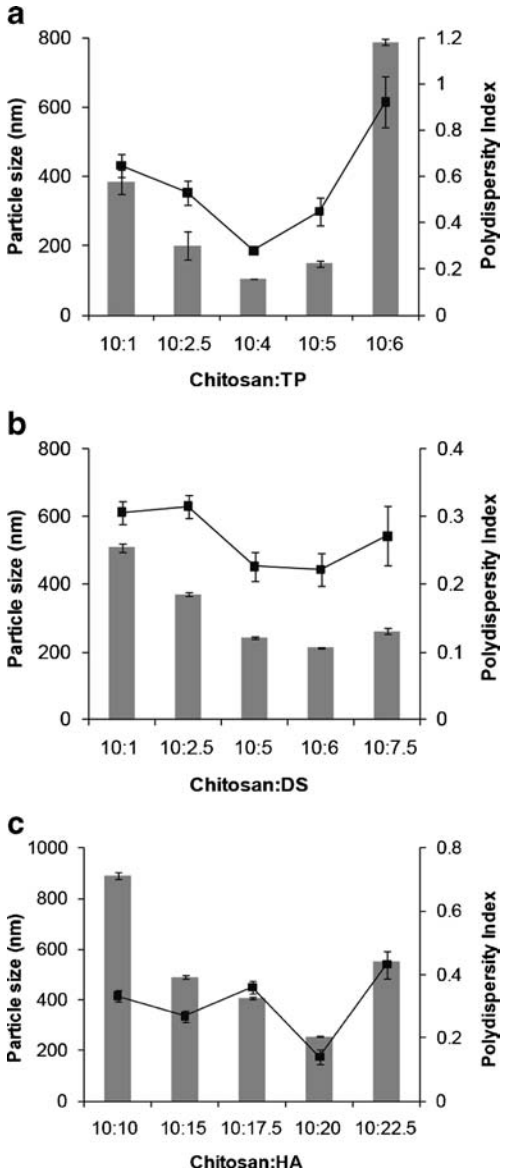

Fig. 1 Effect of the CS:polyanion weight ratio on NP size and PDI. (**a**) CS-TP, (**b**) CS-DS, and (**c**) CS-HA.

accompanying increase in scattering intensity and decrease in particle size (24). However, the addition of excess polyanion led to clear flocculation of NPs with a dramatic increase in the size and dispersity of the nanosuspensions (9). This phenomenon is attributed to the neutralization of all the surface charges on the CS polymer resulting in the loss of potential cross-linking sites, leading to the formation of a single large NP upon further addition of multivalent counter ions (25). All the NP dispersions went through three stages during the formation of stable complexes: clear solution (low concentration of polyanion), slight-medium opalescence (optimum polyanion concentration), and flocculation (excess polyanion).

From our results, it can be inferred that specific polymer ratios were required to maintain the intermolecular distance and cross-linking/gelation density (15). Thus, 10:4, 10:6, and 10:20 of CS-TP, CS-DS, and CS-HA, respectively were found to be suitable weight ratios to generate a colloidal shape or stable NP system.

Effect of Polymer Ratio on ζ-Potential

Figure 2 illustrates the effect of the CS:polyanion weight ratio on the ζ-potential of the resulting CS-NPs. As can be seen, the net positive charge of all the CS-NPs gradually decreased with an increased polyanion ratio. Generally, the long- and short-

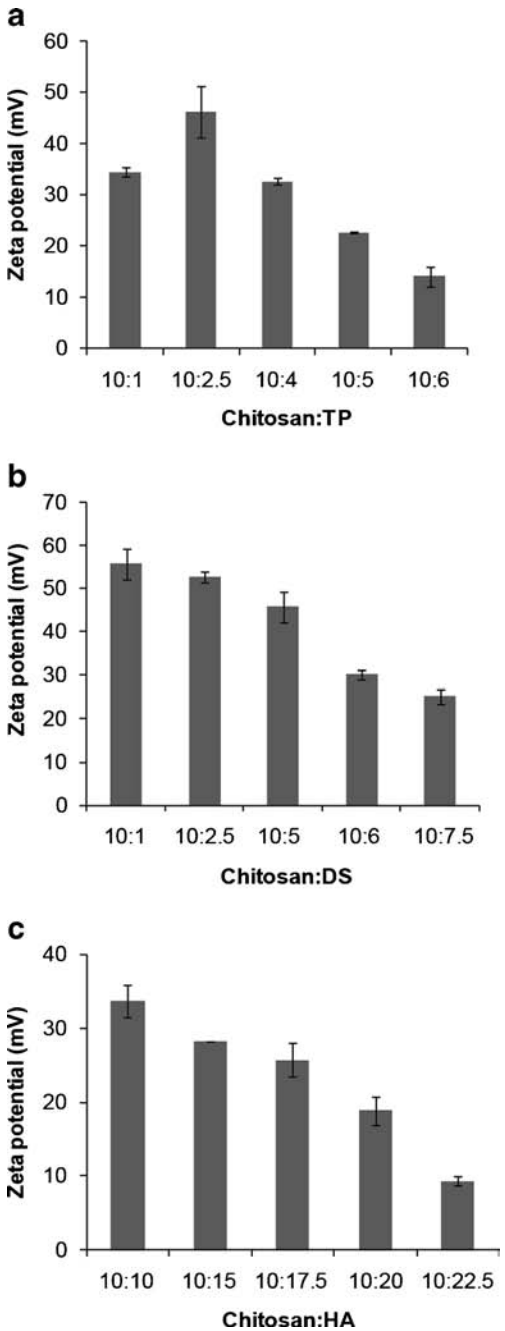

Fig. 2 Effect of the CS:polyanion weight ratio on ζ-potential. (**a**) CS-TP, (**b**) CS-DS, and (**c**) CS-HA.

term stability of NP dispersions are strongly dependent upon the surface electric bi-layer (ζ-potential) (5). The small polyanions can penetrate inter- and intramolecular spaces between the CS molecules, neutralizing the overall charge density on the chain. Consequently, as long as the particles have sufficient repulsive force (+/−25±5 mV) to resist coalescence or flocculation, NPs remain colloidally stable (15). At higher TP, DS, or HA concentrations, the net surface charge dropped below this 25 mV threshold value, which could have triggered agglomeration. Interestingly, the surface charge on CS-HA NPs remained largely constant until a CS:HA weight ratio of 10:10. However, after that point the charge suddenly decreased. This could be due to the inability of the single ionizing HA group to neutralize the multiple charges on the CS residue at lower concentrations (26). In contrast, TP and DS could counter the strong positive charge even at lower concentrations, due to their multiple phosphates and sulfate groups. The proportional reduction in particle size along with the decrease in surface charge was due to the consumption of protonated amine functional groups, resulting in the formation of condensed NPs (13, 27). On the other hand, the surface charge at the optimal polymer ratios (producing the smallest NPs) was between 20 and 30 mV, reflecting a strong dispersion stability. In addition, the positive charge of all the NPs strongly suggested that CS was on the surface, with the counter ion inside due to their smaller size. This positive charge will facilitate NP cellular transport and adhesion (25).

DOX-Loaded CS-NPs

DOX-loaded CS-NPs (CS-TP/DOX NPs, CS-DS/DOX NPs and CS-HA/DOX NPs) were prepared by mixing polyanion solution with the CS solution containing DOX. The entrapment of DOX in the CS-based NPs system was clearly evident from the increased particle size and ζ-potential (Table I). The particle sizes of DOX-loaded CS-NPs were 10–20 nm higher than the respective blank CS-NPs due to the electrostatic accommodation of DOX in the CS-NPs. The PDI across all optimized complexes was well below the optimum range for mono-dispersion. The incorporation of DOX into CS-NPs resulted in a marginal increase of ζ-potential, due to the positive charge contributed by the drug.

The entrapment efficacy of DOX in CS-NPs decreased with increasing drug concentration (Fig. 3). At a low drug concentration, the entrapment efficacy was higher because of the abundant charge available for interaction on the polyanion, facilitating efficient incorporation within the NPs. At a higher drug concentration, however, the number of charged species and overall polyanion charge density were saturated by DOX. For this reason, increasing the drug concentration did not produce any additional encapsulation within the NPs.

Moreover, the CS-DS/DOX NPs and CS-TP/DOX NPs exhibited a relatively higher DOX entrapment than CS-HA/DOX NPs, although there was no statistically significant difference between the three systems. Overall, a high entrapment of more than 50% in all the NPs tested suggested efficient entrapment in PEC NPs. Furthermore, the loading capacity of each NP system varied due to the polyanion charge differences. The loading capacities of CS-TP/DOX NPs, CS-DS/DOX NPs, and CS-HA/DOX NPs were 40% w/w, 37.5% w/w, and 18.7% w/w, respectively. The low loading capacity in CS-HA/DOX NPs was attributed to its low charge density that consumed relatively more HA moiety per chitosan block to form a stable NP, thus increasing the weight percentage of NP mass per DOX molecule.

Interestingly, the entrapment efficiency was only around ~25–30% when DOX was added to preformed CS NPs (data not shown). The low entrapment efficacy achieved using this method may be due to a weaker electrostatic interaction between DOX and polyanion caused by a reduced charge density resulting from the neutralization of cationic and anionic species. In contrast, when polyanions were added to the DOX/CS mixture, competitive binding occurred, resulting in the formation of stable NPs with higher entrapment efficacies. As polyanions have multiple charged functional groups, the same polymer block can interact with both DOX and CS, resulting in shielding and electrostatic interactions. Furthermore, the comparatively low molecular weight anionic molecules (1,000–5,000 Da) become interspersed between the large CS chains, resulting in the consumption of protonated amine functional groups and the formation of condensed NPs.

Table I Characterization of CS-Based NPs

	Blank CS-NPs			DOX-loaded CS-NPs		
	CS-TP	CS-DS	CS-HA	CS-TP/DOX	CS-DS/DOX	CS-HA/DOX
Size (nm)	105.3 ± 1.5	212.7 ± 2.3	256.0 ± 11.2	123.8 ± 12.8	255.5 ± 11.1	271.3 ± 7.0
PDI	0.279 ± 0.011	0.221 ± 0.024	0.140 ± 0.031	0.363 ± 0.019	0.228 ± 0.021	0.216 ± 0.003
ζ-potential (mV)	22.6 ± 0.1	30.2 ± 1.1	18.9 ± 1.5	29.9 ± 0.6	32.6 ± 0.5	24.5 ± 1.0

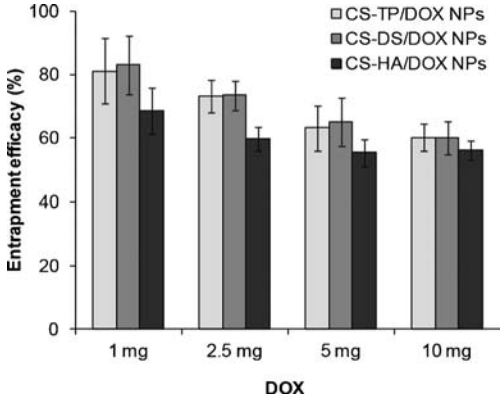

Fig. 3 Effect of DOX concentration on entrapment efficiency in CS-NPs.

Morphology Analysis

TEM imaging confirmed the CS-NP sizes in the dried state along with providing information on their structural morphology after negative staining (Fig. 4). The TEM image of CS-TP NPs showed clearly distinguishable mono-dispersed spherical particles (Fig. 4a). These showed good particle integrity indicating strong interactions between CS and TP. The larger particles are either particle clusters or conglomerates formed after solvent evaporation. CS-DS NPs were almost perfectly spherical (Fig. 4b). The darker cores in CS-TP NPs and CS-DS NPs may be attributed to high electron density, as phosphate and sulfate have higher electron density than CS (15). CS-HA NPs also presented a well-defined spherical morphology (Fig. 4c). Overall, all the NPs were smaller than DLS measurements had indicated. This discrepancy in size data was because of the fact that DLS provided hydrodynamic size in the swollen state, whereas TEM provided the diameter in the dried state.

Figure 4d–f indicate that DOX-loaded CS-NPs retained particle integrity, suggesting that this drug was satisfactorily incorporated into the NP system. The DOX-loaded CS-NPs were slightly larger than the unloaded CS-NPs, consistent with the DLS results. A slight aggregation of CS-HA/DOX NPs may have been due to hydrogen bonding interactions between particles, which gradually became stronger during the drying process.

Physical Characterization

FTIR spectral analysis reveals the chemical interactions between drug and polymer functional groups. FTIR spectra of free DOX and DOX-loaded CS-NPs are presented in Fig. 5a. DOX exhibited characteristic peaks at 3,520 cm^{-1}, 3, 330 cm^{-1}, 2,920 cm^{-1}, 1,750 cm^{-1}, 1,610 cm^{-1}, 1,450 cm^{-1}, 1,280 cm^{-1}, 1,070 cm^{-1}, and 875 cm^{-1}, corresponding to N-H^{v}, O-H, C-H, C-O, N-H$^{\delta}$, C-C, C-O-C, C-O, and N-H^{w} stretching vibrations, respectively. In particular, peaks at 3,520 cm^{-1} and 3,330 cm^{-1} corresponded to N-H stretching vibrations of the primary amine group

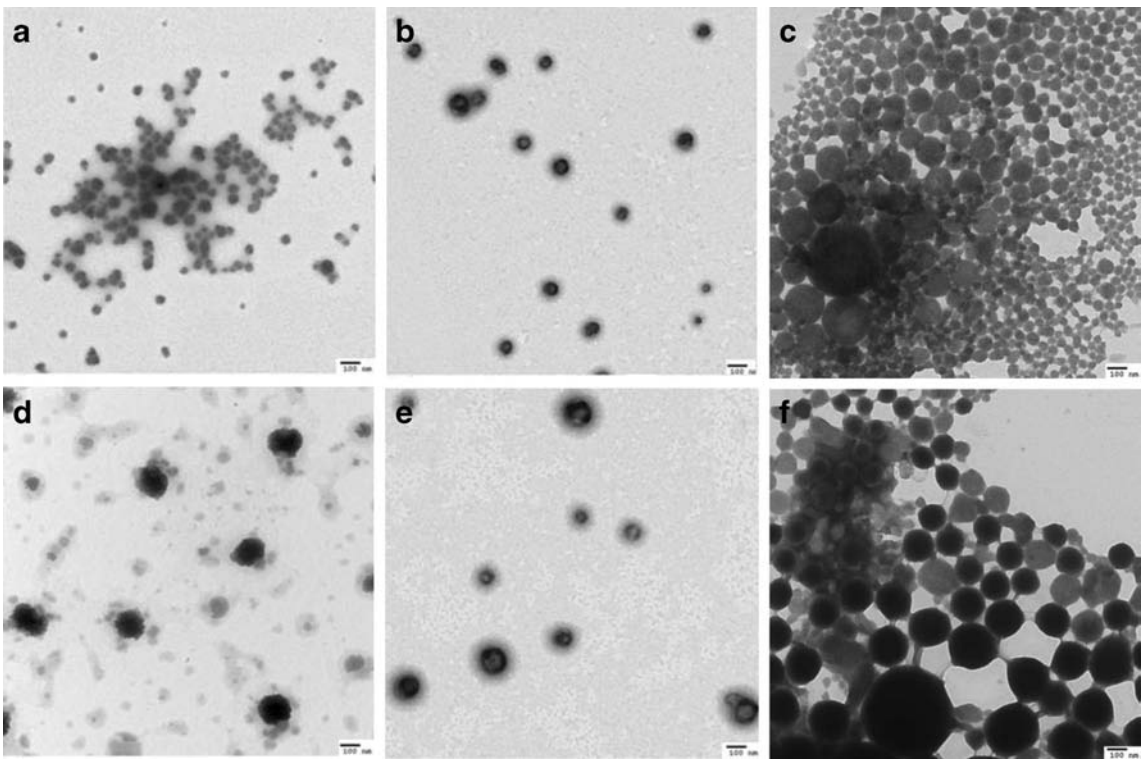

Fig. 4 TEM images of (**a**) CS-TP NPs, (**b**) CS-DS NPs, (**c**) CS-HA NPs, (**d**) CS-TP/DOX NPs, (**e**) CS-DS/DOX NPs, and (**f**) CS-HA/DOX NPs.

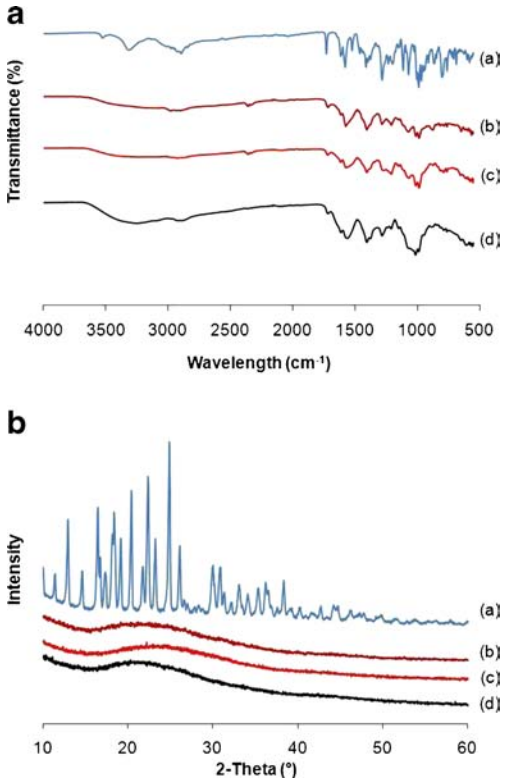

Fig. 5 (**a**) FTIR spectra and (**b**) XRD patterns of (*a*) free DOX, (*b*) CS-TP/DOX NPs, (*c*) CS-DS/DOX NPs, and (*d*) CS-HA/DOX NPs.

and O-H stretching vibrations (28). However, in DOX-loaded CS-NPs these peaks were overlapping, broadened and slightly shifted to a lower frequency range (~3,250 cm^{-1}). In addition, bands at 875 cm^{-1} (due to N-H wag in pure DOX) also diminished. From the FTIR spectra it can be inferred that DOX bound to CS-TP NPs, CS-DS NPs, and CS-HA NPs via an interaction between its protonated $–NH_2$ group and the polymers.

The dispersion stability of NPs strongly depends upon the nature of the drug incorporated. An amorphous drug prevents the Ostwald ripening phenomenon, leading to a stable NP dispersion. XRD patterns of free DOX and DOX-loaded CS-NPs are presented in Fig. 5b. The DOX XRD diffractogram showed numerous sharp and intense peaks at various 2θ scattered angles, reflecting its highly crystalline nature. The peaks corresponding to the native drug crystals were observed at 2θ scattered angles of 13.4°, 15.2°, 17.2°, 20.8°, 22.3°, 26.5°, 27.4°, and 30.5°. However, the complete absence of such characteristic peaks in XRD diffractograms of DOX-loaded CS-NPs suggested a typical amorphous pattern.

In Vitro Drug Release

The release profiles of the three DOX-loaded CS-NP systems are depicted in Fig. 6. Two distinct phases were seen, with almost 20% DOX released within 2 h, followed by 40–70% released over the remaining time period (up to 24 h) at physiological pH (Fig. 6a). This burst release may be attributed to loose electrostatic binding of drug with the respective polymer. Interestingly, DOX release from CS-DS/DOX NPs was much slower and more sustained at the end of the 24 h study, whereas approximately 70% of drug had been released from CS-HA/DOX NPs by this stage. This result clearly indicated the strong DOX binding affinity with the multiple sulfate groups in the DS polymer. The faster release of DOX from CS-HA/DOX NPs was consistent with its relatively lower binding affinity for HA, responsible for the disassembly of nano-architecture. Free DOX was tested as a control and released 100% within 6 h, indicating that the dialysis membrane did not impede DOX release.

We performed an additional release study under acidic conditions as these are often present within tumors and a delivery system with a pH-dependent release profile would be invaluable for tumor drug delivery. DOX release rates from the three different CS-NPs were significantly augmented at pH 5.0, as compared to physiological pH 7.4 (Fig. 6b–d). The increased release of drug cargo from the NPs under acidic conditions might be attributed to (a) the protonation of anionic polymers, decreasing the ionization potential and charge density to interact with the CS amino groups, resulting in NP structure destabilization (29); (b) increased solubility of DOX, which is a base (pKa = 8.2) (30); and (c) CS swelling due to strong protonation of its amine functional group, which may facilitate faster drug elution (6). This *in vitro* release study therefore demonstrated that DOX release from the CS-NPs was sustained over 24 h and that it was more effective at an acidic pH. Additionally, none of the formulations underwent aggregation and remained very stable for at least 3 months at 4°C (Fig S1).

To describe the kinetics of DOX release from DOX-loaded CS-NPs, the *in vitro* release data were mathematically fitted to three commonly used models; Higuchi's model, first order, and zero order (31, 32). The goodness-of-fit for each model was ranked in the order of Higuchi > first order > zero order (Table S1), and diffusion seemed to be the primary factor controlling the release of drug from the NP systems. For Higuchi's model, the 24 h DOX release profile was plotted against the square root of time (Fig. S2). This Higuchi plot showed good linearity for all the NPs tested throughout the 24 h study period, indicating a controlled release phenomenon. Furthermore, the rate constant K calculated from the Higuchi plot provided a good indicator of the release kinetics (33). CS-DS/DOX NPs had the lowest rate constant, suggesting a slow and controlled release profile. To characterize the differences between the NP release profiles in more detail, data were fitted to the Korsmeyer-Peppas equation, where exponent 'n' is indicative of the release mechanism. An exponent value of $n < 0.45$ indicates a Fickian diffusion, n between 0.45 and 0.89 would indicate non-Fickian diffusion (anomalous transport), $n = 0.89$ indicates a purely

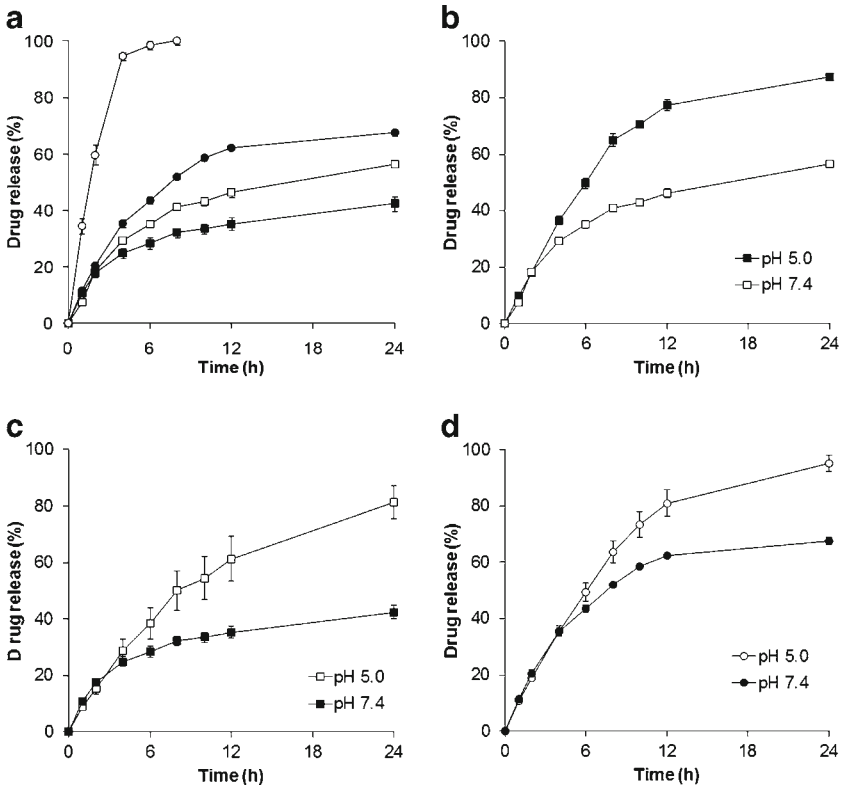

Fig. 6 (**a**) *In vitro* release of DOX from DOX-loaded CS-NPs at pH 7.4. Free DOX (*white circle*), CS-TP/DOX NPs (*white square*), CS-DS/DOX NPs (*black square*), and CS-HA/DOX NPs (*black circle*). *In vitro* release of DOX from (**b**) CS-TP/DOX NPs, (**c**) CS-DS/DOX NPs and (**d**) CS-HA/DOX NPs at pH 5.0 and 7.4.

relaxed controlled delivery, and $n > 0.89$ would indicate super case II transport (34). In the present study, for all the NP formulations tested, n ranged between 0.45 and 0.7, suggesting that more than one mechanism was responsible for DOX release from the NP system and corresponds to non-Fickian kinetics. Thus, DOX release might be a combination of both diffusion and polymer relaxation.

Cellular Uptake and Cytotoxicity Assay

The intracellular accumulation of DOX was compared in MCF-7 and A-549 cell lines exposed to DOX-loaded CS-NPs for 2 h (Fig. 7). In MCF-7 cells, DOX uptake was higher from CS-HA/DOX NPs than CS-DS/DOX NPs or CS-TP/DOX NPs. This may reflect HA binding to CD44 receptors present on the MCF-7 cell surface, increasing cellular uptake of the CS-HA/DOX NPs, as CD44 acts as the primary cell surface receptor for HA internalization and turnover (35, 36). Although similar cellular uptake patterns were observed in A-549 cells, the total DOX concentration was slightly lower than in the MCF-7 cells. CD44 is highly expressed in both MCF-7 and A-549 cells. The relative median fluorescence intensity, corresponding to the level of CD44 expression, did not differ significantly between the cell lines. It has been shown that the intracellular delivery of various HA-based nanocarriers was facilitated in MCF-7 or A-549 cell lines expressing high levels of CD44 (37–39). Thus, the higher cellular uptake of CS-HA/DOX NPs might be attributed to the higher binding affinity of HA derivatives to CD44, increasing receptor-mediated endocytosis (40).

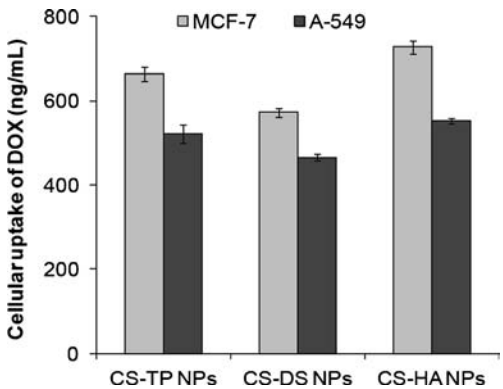

Fig. 7 *In vitro* cellular DOX uptake studies in MCF-7 and A-549 cells incubated with CS-TP/DOX NPs, CS-DS/DOX NPs, or CS-HA/DOX NPs for 2 h.

The cytotoxicity of blank CS-TP NPs, CS-DS NPs, and CS-HA NPs in MCF-7 and A-549 cells were analyzed (Fig. 8a). Blank CS-HA NPs were very compatible with both cell lines, with viability remaining above 90% at all concentrations tested (0.1–500 μg/mL). This was consistent with the fact that HA is a naturally occurring biocompatible polymer and a main component of the extracellular matrix. MCF-7 and A-549 cells also showed high levels of viability in the presence of CS-DS NPs and CS-TP NPs, but these NPs were slightly cytotoxic at the highest concentration tested. It was previously reported that CS was cytotoxic to some cell lines.

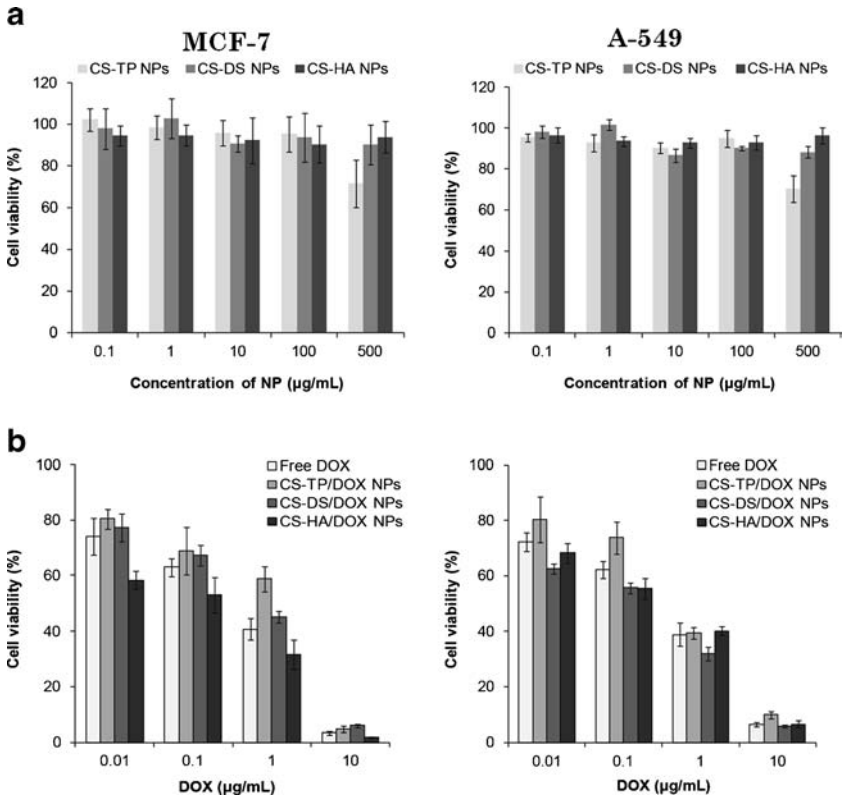

Fig. 8 *In vitro* cytotoxicity of (**a**) blank CS-NPs and (**b**) DOX-loaded CS-NPs against MCF-7 and A-549 cells after a 24-h exposure. The data are presented as mean ± SEM ($n = 8$).

However, the negligible toxicity of the CS-NPs tested in the present study may relate to the inclusion of biocompatible polymers (HA, DS and TP) in the nanostructure (41).

We next investigated the cytotoxic effects of DOX-loaded CS-NPs on the MCF-7 and A-549 cell lines (Fig. 8b). It was evident that CS-HA/DOX NPs were more cytotoxic to MCF-7 cells than either free DOX or the other CS-NPs tested. Free drug would usually exhibit more prominent actions than the same drug incorporated into a NP, due to slower release from the NP. The increased cytotoxicity of CS-HA/DOX NPs in the present study was consistent with the data showing greater internalization into MCF-7 cells, described above. Furthermore, it has been reported that HA binding with the CD44 receptor triggers a cascade of cellular signaling processes (42) that could in turn promote the cytotoxicity of the loaded drug. Our *in vitro* release study indicated that DOX release from CS-HA/DOX NPs was markedly faster than DOX release from the other two NP systems tested. In addition, DOX release rates from the three CS-NPs were significantly augmented at pH 5.0, as compared to physiological pH 7.4 (Fig. 6). Most of the DOX from all three CS-NPs was released over 24 h at pH 5.0. Therefore, during

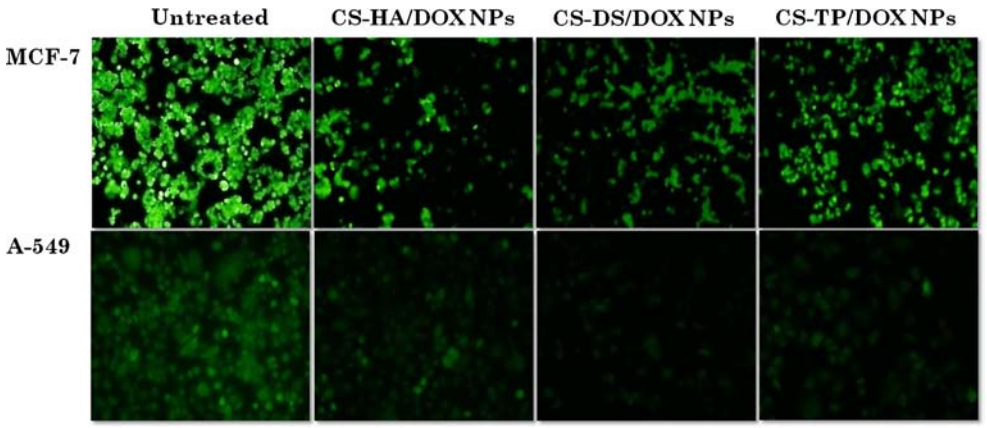

Fig. 9 Fluorescence microscopy pictures of metabolically active MCF-7 and A-549 cells (*calcein green*) following exposure to DOX-loaded CS NPs for 6 h.

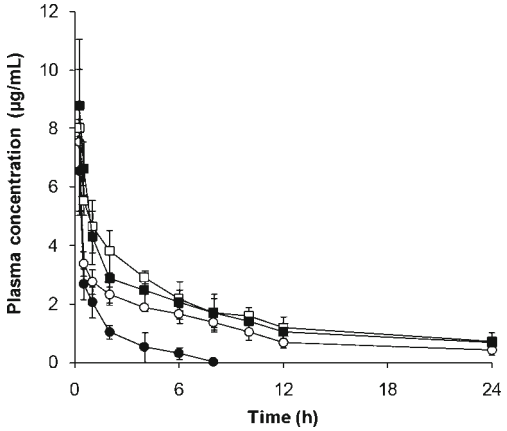

Fig. 10 Plasma concentration-time profiles of DOX after intravenous administration of free DOX (*black circle*), CS-TP/DOX NPs (*white square*), CS-DS/DOX NPs (*black square*), and CS-HA/DOX NPs (*white circle*) to rats at a dose of 10 mg/kg. Each value represents the mean ± S.D. ($n = 3$).

24 h incubation with cells, a sustained release phenomenon maintained an effective concentration of the drug at the target site. CS-HA/DOX NPs, with a relatively faster release pattern and higher cellular uptake, were more cytotoxic than CS-DS/DOX NPs or CS-TP/DOX NPs, and were associated with greater accumulation of drug in the nucleus. The lower cytotoxic effects of CS-DS/DOX NPs and CS-TP/DS NPs were consistent with their more sustained drug release pattern. However, since the cells were incubated with drug for 24 h, *in vitro* cytotoxicity might also be affected by pH-sensitive release from these systems after uptake into the cell lines via endocytosis. The results indicated that the cytotoxic effects in MCF-7 cells followed the order: CS-HA/DOX > CS-DS/DOX > CS-TP/DOX NPs. This trend was similar in A-549 cells, although the CS-DS/DOX NPs were equally or slightly more cytotoxic than CS-HA/DOX NPs in this cell line. Notably, CS-TP/DOX NPs were less cytotoxic than free DOX in both cell lines.

We also used the Live/Dead assay kit to provide a qualitative measure of cell viability after exposing the cell lines to DOX-loaded NPs for 6 h. Figure 9 shows these data, with untreated cells as a control representing 100% live (green) cells. MCF-7 cells showed marked differences in the extent of reduction in green cells following treatment with the three different NP systems. A-549 cells showed no clear distinction between the NPs tested (Fig. 9). The change in cell morphology after the treating with DOX-loaded CS-NPs is shown in Fig. S3.

Pharmacokinetic Study

The plasma concentration-time profiles of DOX following single dose intravenous (IV) administration are presented in Fig. 10. Free DOX, CS-TP/DOX NPs, CS-DS/DOX NPs, or CS-HA/DOX NPs were administrated at a dose of 10 mg/kg via the femoral vein. Free DOX was rapidly cleared from the circulation within 6 h of IV administration and exhibited linear pharmacokinetics. As reported previously, the linear pharmacokinetic profile of DOX remained the same whether administered at high (16 mg/kg) or low (4 mg/kg) starting dose (37, 43). In contrast, DOX had a remarkably prolonged plasma circulation time after administration of CS-TP/DOX NPs, CS-DS/DOX NPs, or CS-HA/DOX NPs and maintained a therapeutic drug level throughout the study period. The corresponding pharmacokinetic parameters are presented in Table II. All the CS-NPs tested demonstrated improved DOX retention in the blood and elevated total plasma concentrations, compared to administration of free DOX. For instance, the AUC of DOX from CS-TP/DOX NPs was approximately 7-fold greater than that of free DOX. The effective elimination half-life ($t_{1/2}$) of CS-TP/DOX NPs was approximately 9-fold longer than that of free DOX, while drug clearance decreased 9-fold. In particular, DS and TP-based NPs were relatively more stable and produced a better DOX pharmacokinetic profile than the HA-based NPs. In summary, all the CS NPs remained stable in plasma, exhibiting a prolonged circulation time and maintaining a high plasma concentration for up to 24 h. The anionic polymer interspersed in the CS NPs has anti-fouling properties as a result of the hydrophilic brush-like hydrated layers that can prolong nanoparticle circulation by minimizing protein adsorption and opsonization. These pharmacokinetic patterns were consistent with the *in vitro* sustained release profile and physical stability of these NPs perhaps due to their multiple charge densities providing strong cross-linking with CS, improving plasma stability and producing sustained DOX release.

Table II Pharmacokinetic Parameters of DOX After Intravenous Administration of Free DOX, CS-TP/DOX NPs, CS-DS/DOX NPs, or CS-HA/DOX NPs in Rats

Parameters	Free DOX	CS-TP/DOX NPs	CS-DS/DOX NPs	CS-HA/DOX NPs
C_{max} (µg/ml)	6.54 ± 1.36	8.03 ± 0.30	8.79 ± 2.29	7.55 ± 2.50
K_{el} (h^{-1})	0.97 ± 0.47	0.10 ± 0.01	0.10 ± 0.02	0.10 ± 0.11
$t_{1/2}$ (h)	0.82 ± 0.32	7.64 ± 0.70	6.65 ± 1.35	6.84 ± 1.12
AUC_{all} (h.µg/ml)	7.21 ± 1.14	44.06 ± 2.54	39.37 ± 8.54	27.88 ± 2.93
AUC_{inf} (h.µg/ml)	7.22 ± 1.13	50.49 ± 1.61	48.80 ± 12.59	32.30 ± 4.80
MRT	1.64 ± 0.62	7.93 ± 0.53	10.37 ± 2.68	10.90 ± 2.47

Data are expressed as the mean ± standard deviation (n = 3)

Conclusion

This study demonstrated the successful loading of DOX into PEC-based CS-NPs, which showed changes in their hydrodynamic size and ζ-potential as a function of the different polyanions incorporated and their weight ratios. CS-TP/DOX NPs and CS-DS/DOX NPs exhibited relatively better physical stability and more sustained DOX release than CS-HA/DOX NPs. However, CS-HA/DOX NPs showed a markedly higher cytotoxicity in MCF-7 and A-549 cells, probably due increased uptake facilitated by CD44-mediated endocytosis. Pharmacokinetic data clearly showed that the PEC-based CS-NPs significantly improved DOX plasma circulation time and decreased its elimination rate constant. Specifically, CS-TP/DOX NPs and CS-DS/DOX NPs exhibited better plasma stability than CS-HA/DOX NPs, due to their strong cross-linkage. This study provides a platform to improve the efficiency of drug delivery in the pharmaceutical and biomedical sectors.

ACKNOWLEDGMENTS AND DISCLOSURES

This research was supported by the National Research Foundation of Korea (NRF) grant funded by the Ministry of Education, Science and Technology (No. 2012R1A2A2A02044997 and No. 2012R1A1A1039059).

REFERENCES

1. Janes KA, Fresneau MP, Marazuela A, Fabra A, Alonso MJ. Chitosan nanoparticles as delivery systems for doxorubicin. J Control Release. 2001;73:255–61.
2. Lankalapalli S, Kolapalli VRM. Polyelectrolyte complexes: a review of their applicability in drug delivery technology. Indian J Pharm Sci. 2009;71:481–7.
3. Bhattarai N, Gunn JJ, Zhang M. Chitosan-based hydrogels for controlled, localized drug delivery. Adv Drug Deliv Rev. 2010;62:83–99.
4. Park JH, Saravanakumar G, Kim K, Kwon IC. Targeted delivery of low molecular drugs using chitosan and its derivatives. Adv Drug Deliv Rev. 2010;62:28–41.
5. Malhotra A, Zhang X, Turkson J, Santra S. Buffer-stable chitosan–polyglutamic acid hybrid nanoparticles for biomedical applications. Macromol Biosci. 2013;13:603–13.
6. Anitha A, Deepa N, Chennazhi KP, Nair SV, Tamura H, Jayakumar R. Development of mucoadhesive thiolated chitosan nanoparticles for biomedical applications. Carbohydr Polym. 2011;83:66–73.
7. Gan Q, Wang T. Chitosan nanoparticle as protein delivery carrier sys-tematic examination of fabrication conditions for efficient loading and release. Colloids Surf B: Biointerfaces. 2007;59:24–34.
8. Ravi Kumar MNV, Muzzarelli RAA, Muzzarelli C, Sashiwa H, Domb A. Chitosan chemistry and pharmaceutical perspectives. J Chem Rev. 2004;104:6017–84.
9. Jonassen H, Kjøniksen AL, Hiorth M. Stability of chitosan nanoparticles cross-linked with tripolyphosphate. Biomacromolecules. 2012;13:3747–56.
10. Songsurang K, Praphairaksit N, Siraleartmukul K, Muangsin N. Electrospray fabrication of doxorubicin-chitosan-tripolyphosphate nanoparticles for delivery of doxorubicin. Arch Pharm Res. 2011;34:583–92.
11. He CB, Hu YP, Yin LC, Tang C, Yin CH. Effects of particle size and surface charge on cellular uptake and biodistribution of polymeric nanoparticles. Biomaterials. 2010;31:3657–66.
12. Liu Z, Jiao Y, Wang Y, Zhou C, Zhang Z. Polysaccharides-based nanoparticles as drug delivery systems. Adv Drug Deliv Rev. 2008;60:1650–62.
13. Koukaras EN, Papadimitriou SA, Bikiaris DN, Froudakis GE. Insight on the formation of chitosan nanoparticles through ionotropic gelation with tripolyphosphate. Mol Pharm. 2012;9:2856–62.
14. Agnihotri SA, Mallikarjuna NN, Aminabhavi TM. Recent advances on chitosan-based micro- and nanoparticles in drug delivery. J Control Release. 2004;100:5–28.
15. Fan W, Yan W, Xu Z, Ni H. Formation mechanism of monodisperse, low molecular weight chitosan nanoparticles by ionic gelation technique. Colloids Surf B: Biointerfaces. 2012;90:21–7.
16. Nasti A, Zaki NM, Leonardis PD, Ungphaiboon S, Sansongsak P, Rimoli MG, *et al*. Chitosan/TPP and chitosan/TPP-hyaluronic acid nanoparticles: systematic optimisation of the preparative process and preliminary biological evaluation. Pharm Res. 2009;26:1918–30.
17. Yousefpour P, Atyabi F, Farahani EV, Sakhtianchi R, Dinarvand R. Polyanionic carbohydrate doxorubicin–dextran nanocomplex as a delivery system for anticancer drugs: in vitro analysis and evaluations. Int J Nanomedicine. 2011;6:1487–96.
18. Almond A. Hyaluronan. Cell Mol Life Sci. 2007;64:1591–6.
19. Duceppe N, Tabrizian M. Factors influencing the transfection efficiency of ultra low molecular weight chitosan/hyaluronic acid nanoparticles. Biomaterials. 2009;30:2625–31.
20. Qadi SA, Meda MA, Zaghloul EM, Taboada P, López CR. Chitosan–hyaluronic acid nanoparticles for gene silencing: the role of hyaluronic acid on the nanoparticles' formation and activity. Colloids Surf B: Biointerfaces. 2013;103:615–23.
21. Haidar ZS, Hamdy RC, Tabrizian M. Protein release kinetics for core-shell hybrid nanoparticles based on the layer-by-layer assembly of alginate and chitosan on liposomes. Biomaterials. 2008;29:1207–18.
22. Bhaskar K, Ravichandiran V, Venkateswarlu V, Rao YM. Lipid nanoparticles for transdermal delivery of flurbiprofen: formulation, in vitro, ex vivo and in vivo studies. Lipids Health Dis. 2009;8:6–18.
23. Ramasamy T, Ruttala HB, Shanmugam S, Umadevi SK. Eudragit-coated aceclofenac-loaded pectin microspheres in chronopharmacological treatment of rheumatoid arthritis. Drug Deliv. 2013;20:65–77.
24. Pedroni VI, Schulz PC, Gschaider ME, Andreucetti N. Chitosan structure in aqueous solution. Colloid Polym Sci. 2003;282:100–11.
25. Huang Y, Lapitsky Y. Salt assisted mechanistic analysis of chitosan/tripolyphosphate micro- and nanogel formation. Biomacromolecules. 2012;13:3868–76.
26. Gan Q, Wang T, Cochrane C, McCarron P. Modulation of surface charge, particle size and morphological properties of chitosan-TPP nanoparticles intended for gene delivery. Colloids Surf B: Biointerfaces. 2005;44:65–73.
27. Oyarzun-Ampuero FA, Brea J, Loza MI, Torres D, Alonso MJ. Chitosan–hyaluronic acid nanoparticles loaded with heparin for the treatment of asthma. Int J Pharm. 2009;381:122–9.
28. Chen Y, Mohanraj VJ, Wang F, Benson HAE. Designing chitosan–dextran sulfate nanoparticles using charge ratios. AAPS PharmSciTech. 2007;8:E98.
29. Kayal S, Ramanujan RV. Doxorubicin loaded PVA coated iron oxide nanoparticles for targeted drug deliver. Mater Sci Eng C. 2010;30:484–90.
30. Barret PC, Gustavsson T, Markovitsi D, Manet I, Monti S. Unravelling molecular mechanisms in the fluorescence spectra of

doxorubicin in aqueous solution by femtosecond fluorescence spectroscopy. Phys Chem Chem Phys. 2013;15:2937–45.
31. Kim JO, Kabanov AV, Bronich TK. Polymer micelles with cross-linked polyanion core for delivery of a cationic drug doxorubicin. J Control Release. 2009;138:197–204.
32. Nogueira DR, Tavano L, Mitjans M, Pérez L, Infante MR, Vinardell MP. In vitro antitumor activity of methotrexate via pH-sensitive chitosan nanoparticles. Biomaterials. 2013;34: 2758–72.
33. Subedi RK, Kang KW, Choi HK. Preparation and characterization of solid lipid nanoparticles loaded with doxorubicin. Eur J Pharm Sci. 2009;37:508–13.
34. Lin LY, Lee NS, Zhu J, Nyström AM, Pochan DJ, Dorshow RB, *et al*. Tuning core vs. shell dimensions to adjust the performance of nanoscopic containers for the loading and release of doxorubicin. J Control Release. 2011;152:37–44.
35. Morrisa GA, Castile J, Smith A, Adams GG, Harding SE. The effect of prolonged storage at different temperatures on the particle size distribution of tripolyphosphate (TPP)–chitosan nanoparticles. Carbohydr Polym. 2011;84:1430–4.
36. Parajó Y, Angelo I, Welle A, Fuente MG, Alonso MJ. Hyaluronic acid/chitosan nanoparticles as delivery vehicles for VEGF and PDGF-BB. Drug Deliv. 2010;17:596–604.
37. Cho HJ, Yoon HY, Koo H, Ko SH, Shim JS, Lee JH, *et al*. Polyethylene glycol-conjugated hyaluronic acid-ceramide self-assembled nanoparticles for targeted delivery of doxorubicin. Biomaterials. 2011;32:7181–90.
38. Lee HJ, Lee K, Park TG. Hyaluronic acid-paclitaxel conjugate micelles: synthesis, characterization, and antitumor activity. Bioconjug Chem. 2008;19:1319–25.
39. Upadhyay KK, Bhatt AN, Mishra AK, Dwarakanath BS, Jain S, Schatz C, *et al*. The intracellular drug delivery and anti tumor activity of doxorubicin loaded poly(γ-benzyl L-glutamate)-b-hyaluronan polymersomes. Biomaterials. 2010;31:2882–92.
40. De la Fuente M, Seijo B, Alonso MJ. Novel hyaluronic acid–chitosan nanoparticles for ocular gene therapy. Investig Ophthalmol Vis Sci. 2008;49:2016–24.
41. Arpicco S, Rosa GD, Fattal E. Lipid-based nanovectors for targeting of CD44-overexpressing tumor cells. J Drug Deliv. 2013:860780.
42. Lu HD, Zhao HQ, Wang K, Lv LL. Novel hyaluronic acid–chitosan nanoparticles as non-viral gene delivery vectors targeting osteoarthritis. Int J Pharm. 2011;420:358–65.
43. Lee HJ, Park WH, Lee MG. Pharmacokinetic and tissue distribution changes of adriamycin and adriamycinol after intravenous administration of adriamycin to alloxan-induced diabetes mellitus rats. Res Commun Mol Pathol Pharmacol. 1995;89:165–78.